A Facile Route to Polymer Solar Cells with Optimum Morphology Readily Applicable to a Roll-to-Roll Process without Sacrificing High Device Performance

By *Hui Joon Park, Myung-Gyu Kang, Se Hyun Ahn,* and *L. Jay Guo**

Photovoltaic cells are being developed as a promising solution to the energy crisis and environmental pollution.[1] Among these, bulk heterojunction (BHJ) polymer photovoltaics have shown strong potential for the production of low-cost, easily processible, and flexible solar cells with acceptable efficiencies.[2–7] As an example, BHJ polymer solar cells can be fabricated by a continuous solution-based roll-to-roll process, as recently demonstrated.[8–10] Polymer BHJ structures, which have been exploited to give the highest efficiencies for polymer photovoltaic (PV) cells, are composed of interpenetrating nanoscale networks of electron donors (e.g., conjugated polymers) and electron acceptors (e.g., soluble fullerene derivatives) with domain sizes on the order of the exciton diffusion length and with large interfacial areas between the domains.[3–7] Such networks can facilitate efficient dissociation of photo-induced excitons at the domain interface. This advantage has made this approach a good candidate for high-efficiency polymer solar cells. However, randomly distributed blend morphologies in BHJ structures inevitably require external treatment to form effective pathways in order for the photogenerated charges to reach each electrode. Accordingly, optimizing the blend morphology to provide effective charge pathways, as well as large interfacial areas, is one of the most crucial issues in the achievement of high efficiency polymer solar cells using BHJ structures.

For this purpose, a number of works, based on poly(3-hexylthiophene):[6,6]-phenyl-C_{61}-butyric acid methyl ester (P3HT:PCBM) as a model system, have reported ways to optimize the BHJ blend morphology. Thermal annealing (TA) and solvent-assisted annealing (SAA) treatments after spin-casting the blend film have become widely accepted as general approaches to control the blend morphology for high-efficiency polymer solar cells, because well-organized interpenetrating networks composed of highly crystallized components can be achieved.[5,6,11] However, recent works that investigated phase separation of components in the vertical direction (i.e., normal to the film and electrode surface) revealed that the BHJ structures fabricated by these methods do not have an optimized morphology: a non-uniform vertical distribution has been observed, with the P3HT phase dominant near the cathode and the PCBM phase dominant near the anode.[12–15] Such a non-uniform distribution is opposed to the ideal solar cell structure, which requires a donor-rich phase near the anode and an acceptor-rich phase near the cathode; such a structure is therefore unfavorable for charge transport to the electrodes. In addition, both annealing processes require relatively long processing times (tens of minutes for TA[5] or a few hours for SAA[6]), and spin-casting deposition can only be applied to small and rigid substrates, making these approaches unsuitable for large areas and hence the mass production of polymer solar cells. Even though high-speed fabrication processes on flexible substrates have been reported, the performances of the resulting devices still cannot compare to those of polymer solar cells based on spin-casting followed by post-treatments.[8–10] This is because the traditional high-speed roll-to-roll coating method may not provide a sufficient annealing time for crystallization and hence results in lower device efficiency.[8–10]

Here, we introduce a novel route that allows evaporation of solvent through surface encapsulation and induced alignment (ESSENCIAL) of polymer chains by applied pressure. The essence of this approach is to utilize a gas-permeable cover layer for solvent evaporation that simultaneously protects the otherwise free surface and induces shear flow of the blend solution by an applied pressure. The process leads to an optimized morphology and more uniform distribution and crystallinity of the components, which is favorable for charge generation and transportation and cannot be achieved by conventional TA and SAA methods. Comparisons between structures fabricated by different methods were made by measuring quantum efficiency, absorbance, X-ray photoelectron spectroscopy (XPS), and hole- and electron-mobilities. Furthermore, the effect of domain features of the components on efficient exciton dissociation was studied using atomic force microscopy (AFM) and photoluminescence (PL). The power conversion efficiency was obtained by charge density–voltage (J–V) measurements based on an isolated cathode geometry in order not to overestimate the efficiency, as has commonly occurred in devices previously reported using cross-bar electrode geometry.[16,17] Our results revealed that this new ESSENCIAL method not only induces much more uniformly distributed interpenetrating continuous pathways having finer nanodomains with high crystallinity, but also is applicable to high-speed dynamic processes, as ultimately demonstrated in a roll-to-roll process preserving high device performances.

[*] H. J. Park, Prof. L. J. Guo
Macromolecular Science and Engineering
The University of Michigan, Ann Arbor, MI 48109 (USA)
E-mail: guo@umich.edu
Dr. M.-G. Kang, Prof. L. J. Guo
Department of Electrical Engineering and Computer Science
The University of Michigan, Ann Arbor, MI 48109 (USA)
S. H. Ahn
Department of Mechanical Engineering
The University of Michigan, Ann Arbor, Michigan 48109 (USA)

DOI: 10.1002/adma.201000250

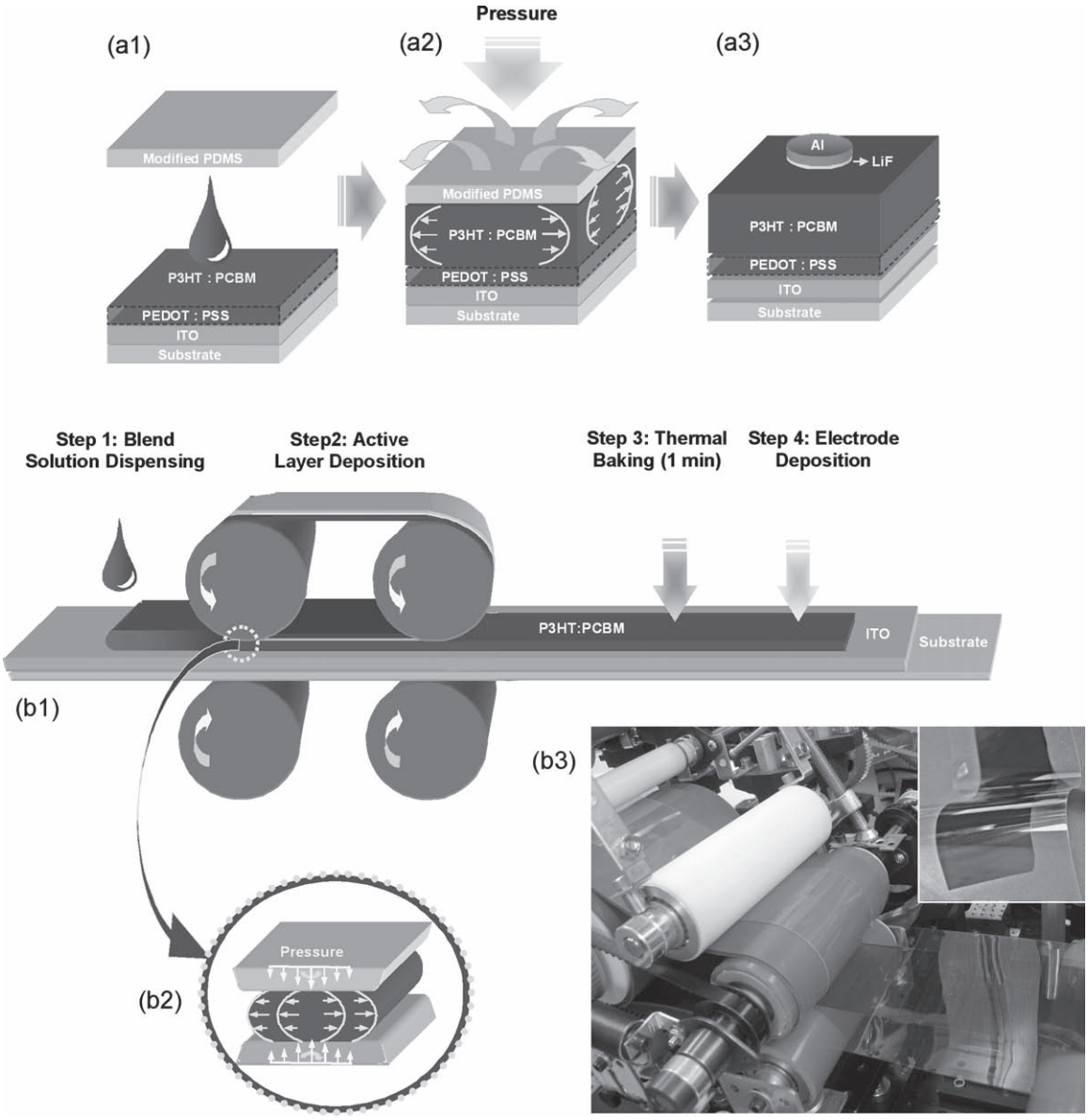

Figure 1. a) Schematic of the ESSENCIAL process for fabricating polymer solar cells: a1) applying blend solution (PDMS and ITO refer to polydimethylsiloxane and indium tin oxide, respectively); a2) active layer formation during solvent evaporation under pressure; and a3) isolated island-type electrode deposition on top of polymer blend film after removing the PDMS stamp. Note that the PEDOT:PSS layer is not indispensable to this processing, as described in the text. b) Roll-to-roll processing for polymer solar cells: b1) schematic of roll-to-roll process for polymer solar cell fabrication; b2) a schematic to depict the squeezed flow behavior of solution during the dynamic roll-to-roll process. The thickness of the liquid coating is affected by the concentration of solution, roller pressure, and rolling speed according to the dynamic elastic contact model;[30] and b3) A photograph of the roll-to-roll apparatus and process (the inset image is the resultant flexible polymer solar cell before electrode deposition).

The ESSENCIAL process is depicted in **Figure 1a**. P3HT:PCBM blends were used as a model system, and the blend solution was placed on a transparent anode substrate and capped with a gas-permeable silicone film, to which pressure was applied. The induced shear flow helped align the polymer chains while the solvent evaporated through the silicone film. The solidified blend layer remained on the substrate after removal of the silicone film. Interestingly, a poly(3,4-ethylenedi oxythiophene):poly(styrenesulfonate) (PEDOT:PSS) layer, widely used on top of transparent anodes in organic PVs, was not indispensable to this processing; this will be further explained later with roll-to-roll application. The thickness of the active layer can be controlled by adjusting the solution concentration and the applied pressure, and the evaporation and solidification time can be reduced to a few seconds by controlling the applied pressure. Detailed information on processing conditions is explained in the Experimental Section.

Firstly, the effects of different processing methods on the crystallinity of the conjugate polymer were investigated by absorbance spectroscopy. The chain ordering of the conjugate

polymer in a BHJ structure is one of the essentials for achieving improved crystallinity for high-efficiency solar cells because the improved organization of polymer chains facilitates hole transport, and the long conjugation length enhances the absorption of light, resulting in efficient exciton generation.[18] Thus, a conjugate polymer with high crystallinity, such as P3HT, is advantageous. The absorption spectrum of the blend film fabricated by the ESSENCIAL method is compared with that made by the spin-casting method in **Figure 2a**. To further evaluate the efficiency of the ESSENCIAL method, samples treated by TA and SAA after spin-casting, which has generally been used to improve the crystallinity of the P3HT, were also examined. A shear stress applied to the polymer solution—which causes organization of the polymer—across the entire depth between two plates is much more effective than that between a plate and an air surface (as, for example, in spin-casting), which decreases continuously from the plate to be zero at the air interface.[19] Therefore, as expected, enhanced vibronic peaks in the absorbance spectra, as well as a significant red-shift indicating a higher degree of ordering of P3HT chains,[20] were observed in the ESSENCIAL sample. Additionally, this processing could be completed in just a few seconds, but the enhancement was found to be much higher than that in samples thermally annealed for 20 min and was even comparable to that of the solvent-assisted annealed sample, in which P3HT crystals were slowly grown for 2 h. This property permits the method to be applied to high speed roll-to-roll processing and can produce well-ordered P3HT domains.

In addition to improved polymer crystallinity, the nanodomains of each blend component should be well-connected in order for holes from charge-separated excitons to be effectively transported to the anode, and the electrons to the cathode, through continuous pathways. However, the non-uniform distribution of the donor and acceptor components found in spin-casted samples, even after TA or SAA, is not helpful for effective charge transport to the electrodes.[12–15] This non-uniform distribution of components in the vertical direction is a consequence of the surface energy difference between P3HT (26.9 J m^{-2}) and PCBM (37.8 J m^{-2}), which pushes P3HT to the low-surface-energy air surface to minimize the overall free energy.[13–15] In contrast, a very uniform vertical distribution is expected for films prepared by the ESSENCIAL process because the gas-permeable silicone film effectively provides a higher surface energy than that of the air surface. The XPS results shown in Figure 2b clearly illustrate these trends. Although the weight ratio of PCBM to P3HT in the blend solution is 1:1, the weight ratio of PCBM to P3HT of thermally and solvent-assisted annealed samples measured at the top surface were 0.411 and 0.488, respectively, which indicates a large accumulation of P3HT at the top. But the ESSENCIAL sample produced a much more balanced value (0.855), which implies a more uniform distribution of components in the vertical direction. In order to confirm that the uniformly distributed components in the ESSENCIAL-treated sample are truly beneficial to effective charge transport by providing more continuous pathways through the film, we constructed hole- and electron-only devices in order to evaluate the charge transport properties in the phase-separated blend film.[21,22] The hole-only device was fabricated by replacing LiF with high-work-function molybdenum oxide (MoO_3) to block the injection of electrons from the Al cathode; the electron-only device was fabricated using low-work-function cesium carbonate (Cs_2CO_3) to replace PEDOT:PSS and to block the hole injection from the ITO anode.[22] Both hole- and electron-mobility were calculated using the space-charge-limited-current (SCLC) model at low voltage:[23]

$$J = \frac{9}{8}\varepsilon_o\varepsilon_r\mu\frac{V^2}{L^3} \quad (1)$$

where $\varepsilon_o\varepsilon_r$ is the permittivity of the component, μ is the carrier mobility, and L is the thickness. As shown Figure 2c1, the hole-mobility of the thermally annealed sample shows the lowest value ($\mu_h \approx 1.57 \times 10^{-4}$ cm^2 V^{-1} s^{-1}) due to relatively poor crystallinity of polymers in such samples. In comparison, the hole-mobility of the ESSENCIAL-treated sample ($\mu_h \approx 1.15 \times 10^{-3}$ cm^2 V^{-1} s^{-1}) was much higher; it was also higher than that of the solvent-assisted annealed sample ($\mu_h \approx 3.29 \times 10^{-4}$ cm^2 V^{-1} s^{-1}), even though the two types of samples showed similar polymer crystallinity in the absorbance measurement (Figure 2a). This means that the uniformly distributed P3HT polymer domains facilitate hole transport, and the most optimized hole-transporting pathways were obtained in the ESSENCIAL sample across the entire depth of the device.

It is known that the insufficient crystallinity of P3HT in the thermally annealed sample is due to the rapidly grown large PCBM crystal domains,[24] which hamper further crystallization of P3HT. However, in the solvent-assisted annealed sample, the mild growth of PCBM provides sufficient time for P3HT to be fully crystallized, leading to much more balanced crystalline morphologies of the two domains.[25] Therefore, contrary to the rapidly grown large aggregation of PCBM which produces poor electron pathways and significantly lower electron-mobility in the thermally annealed sample, the well-balanced PCBM pathway developed in the solvent-assisted annealed sample showed higher electron-mobility ($\mu_e \approx 4.95 \times 10^{-4}$ cm^2 V^{-1} s^{-1}) as shown in Figure 2c2.

An interesting effect was observed for various samples after further TA: for the ESSENCIAL sample, the electron-mobility was drastically increased to the highest value (from 3.61×10^{-7} to 1.46×10^{-3} cm^2 V^{-1} s^{-1}); however, the solvent-assisted annealed sample treated by further TA showed a reduced electron-mobility, similar to that of the thermally annealed sample. We believe that PCBM molecules in the ESSENCIAL sample, which are not well-organized to form efficient electron pathways before TA, are effectively crystallized, and due to the suppression by the uniformly distributed P3HT polymers, are not overgrown into large aggregates even after thermal treatment. Consequently, well-organized PCBM pathways are formed among P3HT polymers to give optimized interpenetrating structures after thermal treatment. However, in the case of the solvent-assisted annealed sample, non-uniformly accumulated PCBM molecules can easily assemble into large PCBM aggregates due to a weaker suppression effect of the P3HT during TA, which inevitably produces poor electron pathways and result in depletion of PCBM in regions within the network structure. Additionally, the effects of further heat treatment were not significant to the hole-mobilities of the solvent-assisted annealed sample (from 3.29×10^{-4} to 2.20×10^{-4} cm^2 V^{-1} s^{-1}) and the ESSENCIAL-treated sample (from

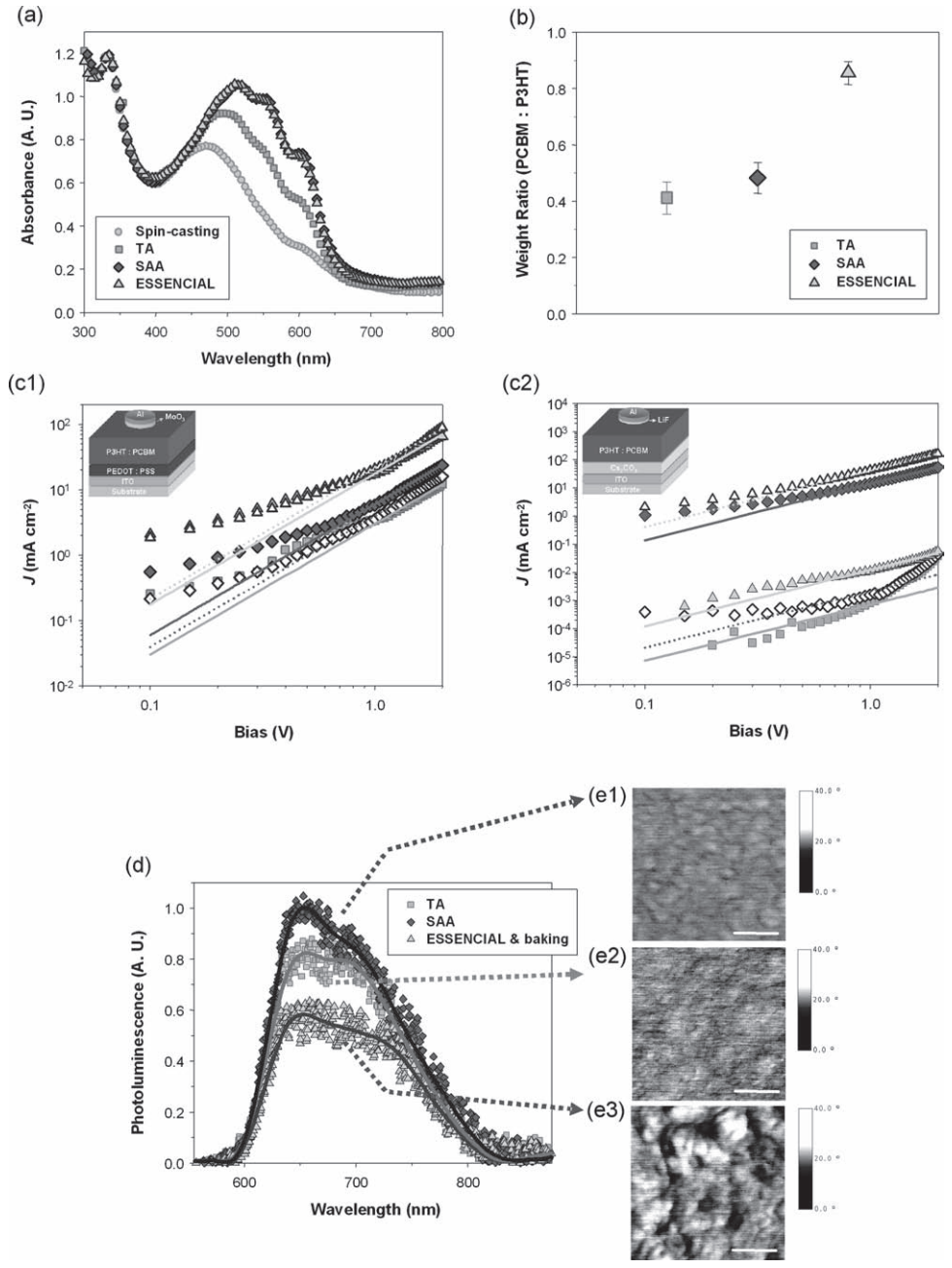

Figure 2. Characteristics of BHJ structures obtained by different processing methods. Circle, square, diamond, and triangle represent the blend films made by spin-casting, TA, SAA, and ESSENCIAL processes, respectively. a) Absorption spectra of the blend films; the spectra have been normalized to the PCBM peak around 325 nm. b) Weight ratio of PCBM to P3HT calculated by XPS results for different processing methods; the error bars represent standard deviations. c) Measured log*J*–log*V* plots under dark conditions for hole- and electron-only devices. The symbols represent experimental data, and the lines are the fit to the experimental data by the SCLC model, showing lines with slope = 2 on the log scale. Open symbols and dotted lines represent further thermally annealed results. The applied bias voltage is corrected for the built-in potential due to the difference in work function of the two electrodes. Insets are schematics of the device structures: c1) hole-only devices and c2) electron-only devices. d) Photoluminescence spectra of blend films. The ESSENCIAL sample was further treated by heat: filled symbols and lines represent experimental data and their polynomial regressions, respectively. e) AFM phase images. The images in e1–e3 correspond to the SAA, TA, and heat-treated ESSENCIAL samples, respectively. The white scale bars represent 50 nm.

1.15×10^{-3} to 1.26×10^{-3} cm^2 V^{-1} s^{-1}) due to sufficiently crystallized P3HTs obtained under both processing conditions (Figure 2c1). Consequently, the most optimized transport pathways for both charge carriers were achieved in the heat-treated ESSENCIAL sample, and well-balanced mobilities ($\mu_e/\mu_h \approx 1.16$) were obtained. Even though the electron-mobilities of the thermally annealed device and the solvent-assisted annealed device with further heat-treatment were not well matched with

Table 1. The calculated carrier mobilities depending on the different processing methods.

	Carrier mobility [10^{-4} cm^2 V^{-1} s^{-1}]		
Method	Electron (μ_e)	Hole (μ_h)	Ratio (μ_e/μ_h)
TA	–	1.57	–
SAA	4.95	3.29	1.50
ESSENCIAL [a]	14.60	12.60	1.16

[a] The ESSENCIAL sample was further treated by heat.

the SCLC model, the significantly lower expected values (10^{-8} to 10^{-7} cm^2 V^{-1} s^{-1}) do not affect any conclusions here. The carrier mobilities depending on different processing methods are summarized in **Table 1**.

As a last aspect, the domain size in the BHJ structures and their effects on the exciton quenching were investigated using AFM and PL, as shown in Figure 2d,e. Compared with the non-uniform mixture, in which one phase is dominant at one surface, more uniformly mixed donor and acceptor phases throughout the film are expected to have finer interpenetrating nanodomains that are advantageous to efficient dissociation of photogenerated excitons, and hence result in suppressed PL from the donor polymer. It has been reported that the PL of annealed samples is enhanced as compared with only spin-casted film, because the higher crystallinity induced by annealing gives a relatively poor exciton dissociation due to the reduction of interfacial area between the donor and acceptor domains.[26] However, the improved charge transport of the annealed samples due to increased crystallinity can offset the poor exciton dissociation effect, still producing high-efficiency solar cells.[27] Therefore, the solvent-assisted annealed sample having higher crystallinity than the thermally annealed sample showed well-defined domains in AFM phase images, and this improved crystallinity induced the enhancement of PL in Figure 2d. As for the heat-treated ESSENCIAL sample, a finer interpenetrating network than the solvent-assisted annealed sample was expected due to the more uniform distribution of the blend, and well-defined nanodomains were much more discernible in AFM phase images. These uniformly distributed and fine interpenetrating nanodomains not only permit good charge pathways, but also facilitate efficient exciton dissociation, therefore suppressing the PL from the donor; consequently this gave the lowest PL in Figure 2d.

The device performances, including power conversion efficiency (PCE) and *J*–*V* curves measured under AM 1.5 G simulated sunlight (at 100 mW cm^{-2} intensity), are summarized in **Figure 3**. In device fabrication, an isolated island-type metallic cathode was used to exclude the overestimation of the photocurrent, as has commonly occurred in devices using cross-bar-type electrodes.[16,17] In our previous report, the PCE could be overestimated by as much as 30%, and perhaps even more depending on the electrode design and measurement conditions.[17] Devices fabricated by the ESSENCIAL method followed by baking showed the highest PCE due to the optimized domain morphologies and charge pathways that resulted in both increased short-circuit current and fill factor (Figure 3c,d). The favorable morphology also led to the lowest series resistance (approximately 1.2 Ω cm^2), as expected. The improvement of PCE was confirmed by improved external quantum efficiency (EQE) in the range of 350–650 nm. Detailed measured values are shown in Figure 3b.

Before advancing towards roll-to-roll fabrication, another remarkable merit of the ESSENCIAL-based device is addressed. PEDOT:PSS is the most widely used buffer layer between an ITO anode and the active organic semiconductor to improve the performances of polymer solar cells. One of the important roles of this PEDOT:PSS layer is to provide efficient electron blocking[28] to prevent electron leakage from the BHJ acceptors.[29] If PEDOT:PSS is not used, our experiments on the annealed devices after spin-casting showed a significant drop in the fill factor (e.g., from 65.1% to 54.8%) that results in much reduction in PCE. However, the ESSENCIAL-based devices showed only a small drop in the fill factor (e.g., from 69.1% to 67.3%), which results in a negligible effect on the PCE. This effect is consistent with the improved morphology in ESSENCIAL devices (discussed above). In the devices with spin-cast film, large amounts of PCBM are non-uniformly assembled near the ITO anode, thereby inducing electron leakage. However, the uniform distribution of components in ESSENCIAL-based devices drastically reduces these electron leakage pathways. This observation alone is important evidence for the uniform distribution of components in the blend film fabricated by ESSENCIAL. Moreover, avoiding the use of PEDOT:PSS can significantly reduce the processing time, as it eliminates the PEDOT:PSS coating and the baking step to remove residual H_2O molecules from PEDOT:PSS used in conventional fabrication; this is especially attractive for high-speed roll-to-roll processing.

The advantages of the ESSENCIAL method to induce a superior BHJ morphology in a short processing time pave the way to scalable high-efficiency polymer solar cell fabrication. Here, we demonstrate fabrication of polymer solar cells using a roll-to-roll apparatus composed of dual rollers and a tensioned belt covered with a gas-permeable silicone film, which enables coating of the polymer blend with a uniform thickness and fast solvent evaporation in a continuous fashion (Figure 1b). According to the dynamic elastic contact model developed for roll-to-roll nanoimprinting[30] (Figure 1b2), the thickness of the coated active layer can be controlled by the solution concentration and roller pressure, as for the small-scale ESSENCIAL experiment discussed earlier, and the film uniformity can be preserved by the belt tension during the solvent evaporation process. Figure 1b3 and the inset image show a three-inch-wide uniform BHJ active layer film made of P3HT:PCBM blend on an ITO-coated PET substrate for flexible solar cells using the continuous roll-to-roll process. After 1 min baking, LiF and Al cathode were deposited, and a PCE (approximately 3.5%) comparable to the small-scale ESSENCIAL experiment was achieved using the roll-to-roll process, as shown in Figure 3.

In conclusion, the novel ESSENCIAL-based technique developed in this work shows a much more optimal BHJ morphology compared with conventional methods. This permits realization of high-efficiency polymer solar cells using a high-speed roll-to-roll process. More importantly, we believe that this new process is equally applicable to BHJ structures using other materials (e.g., the low-bandgap polymer semiconductors that have demonstrated a higher PCE[7]), making it a potential manufacturing

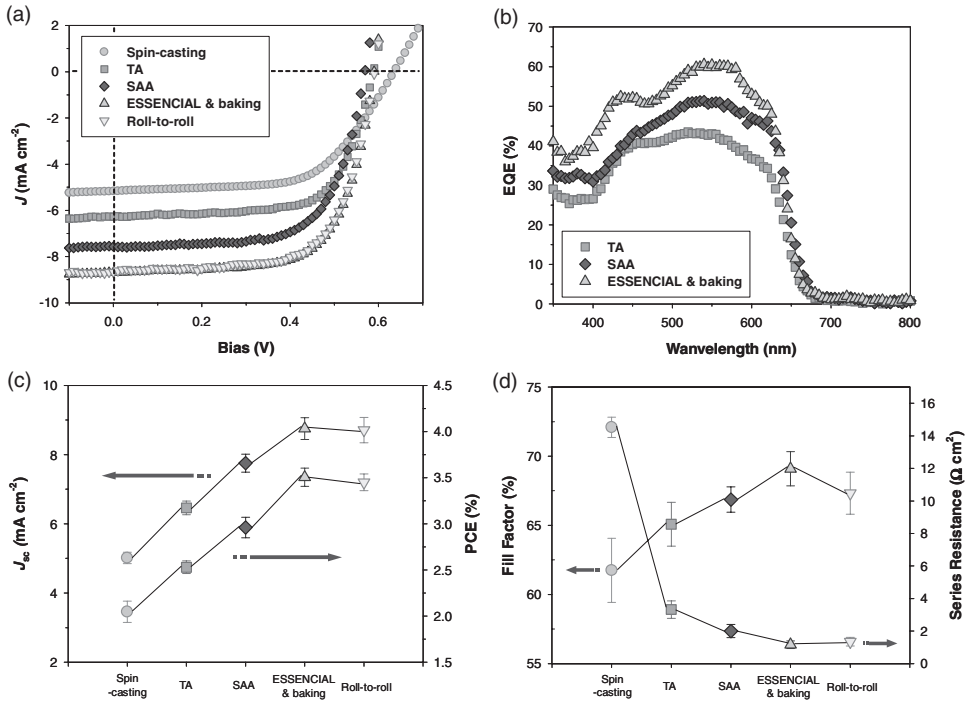

Figure 3. Device performances depending on different processing methods. Symbol are as in Figure 2, with the inverse triangle symbol added for devices made by the roll-to-roll process. All data were measured at AM 1.5 G with an intensity of 100 mW cm^{-2}. a) *J–V* plots. b) External quantum efficiency. c) Power conversion efficiency (PCE) and short-circuit current density (J_{sc}). The error bars represent standard deviations. d) Fill factor (FF) and series resistance (R_s). Average solar cell characteristics are summarized as follows: spin-casting, J_{sc} = 5.01 mA cm^{-2}, V_{oc} (open-circuit voltage) = 0.64 V, FF = 61.7%, R_s = 14.5 Ω cm^2, PCE = 2.05%; thermal annealing, J_{sc} = 6.46 mA cm^{-2}, V_{oc} = 0.60 V, FF = 65.1%, R_s = 3.3 Ω cm^2, PCE = 2.53%; solvent-assisted annealing, J_{sc} = 7.75 mA cm^{-2}, V_{oc} = 0.57 V, FF = 66.9%, R_s = 2.0 Ω cm^2, PCE = 2.96%; heat-treated ESSENCIAL, J_{sc} = 8.75 mA cm^{-2}, V_{oc} = 0.59 V, FF = 69.1%, R_s = 1.2 Ω cm^2, PCE = 3.50%; and roll-to-roll, J_{sc} = 8.71 mA cm^{-2}, V_{oc} = 0.59 V, FF = 67.3%, R_s = 1.4 Ω cm^2, PCE = 3.45%. The solar cells fabricated by roll-to-roll processing were prepared without a PEDOT:PSS layer.

technique for mass production of low-cost, high-efficiency polymer solar cells.

Experimental Section

Device Fabrication: Polymer PV cells had the following planar configuration: transparent substrate/ITO/PEDOT:PSS/P3HT:PCBM/LiF/Al. ITO-coated substrates (Delta Technologies, LTD) were cleaned in acetone and then isopropyl alcohol (IPA) under sonication for 20 min and treated by O_2 plasma for 60 s. Cleaned substrates were then transferred to a N_2-purged glovebox, and the filtered PEDOT:PSS (H. C. Starck, Clevios PH 500) was spin-cast onto the ITO electrodes to deposit an approximately 45 nm thick layer, which was subsequently baked at 115 °C for 15 min. For the active layer, P3HT (Rieke Metals Inc., 4002-E, approximately 91% regioregularity) and PCBM (American Dye Source, Purity: >99.5%) were used as received, and blend solutions were prepared by dissolving both components in 1,2-dichlorobenzene at a 1:1 ratio (w/w). The solution was stirred for approximately 12 h in the N_2-purged glovebox to give a homogeneous blend system and filtered using a 0.45 μm filter.

The thermally annealed devices were fabricated by spin-casting blend solution onto the PEDOT:PSS layer for 90 s and subsequent annealing at 130 °C for 20 min. After thermal treatment, LiF (1 nm) and Al (80 nm) electrodes were deposited by thermal evaporator at a pressure of 8×10^{-7} mbar through circularly shaped shadow masks of 3.5 mm diameter. For the solvent-assisted annealed devices, the spin-casting time was reduced to 30 s to retain a certain amount of residual solvent in the blend film, and the sample was immediately covered by a glass petri dish to slowly evaporate the solvent for 2 h. The ESSENCIAL process was performed by squeezing the blend solution between a modified PDMS silicone film that is gas-permeable and solvent-resistant with minimal deformation[31] and an ITO substrate coated with PEDOT:PSS. After separating the silicone film, the blend film was baked at 130 °C for 1 min before further electrode deposition. The effects of 1–20 min thermal treatment times on the device performances of the ESSENCIAL-treated samples were consistent. The thickness of the blend film fabricated by the ESSENCIAL method was controlled by changing the concentration of P3HT:PCBM solution (from 0.2 wt%/0.2 wt% to 4 wt%/4 wt%) and the applied pressure (from 0.1 to 20 psi), and the solvent evaporation time was changed from tens of minutes to a few seconds, depending on the applied pressure. We did not find any significant differences in the performances of the ESSENCIAL-based devices having the same thickness but were fabricated using different conditions such as the concentration of solution, applied pressure, or processing time. Every device fabricated in this work has an approximately 240 nm thick active layer, as measured by a Dektek profiler. To confirm the effect of PEDOT:PSS layer on the device performances, O_2-plasma-treated ITO substrates were also used to substitute the PEDOT:PSS/ITO substrate.

Hole-only devices had the structure: transparent substrate/ITO/PEDOT:PSS/P3HT:PCBM/MoO_3/Al. After following the processes mentioned above, deposition of 20 nm of MoO_3 onto the active layer instead of LiF and Al deposition through the shadow mask completed device fabrication. Electron-only devices had the structure: transparent substrate/ITO/Cs_2CO_3 /P3HT:PCBM/LiF/Al. Cs_2CO_3 (0.2 wt%), dissolved in 2-ethoxyethanol, was spin-cast on ITO substrate and subsequently baked at 170 °C for 20 min. The remaining procedures, such as active layer deposition and cathode deposition, were chosen according to the type of processing.

Device Performance Measurements: Current versus voltage characteristics were measured with an HP4156B semiconductor analyzer by illuminating the polymer PV cells with AM 1.5 G simulated sunlight using an Oriel Solar Simulator at an irradiation intensity of 100 mW cm^{-2}, which was calibrated by a power meter (OPHIR, Nova-Oriel) and a reference silicon solar cell. Incident-photon-to-collected-charge-carrier efficiency (IPCE) spectra for EQE were measured with a 150 W Oriel Solar Simulator light source, an Acton Research Corp. Spectra-Pro 275 monochromator, a chopper wheel and a Stanford Research 830 lock-in amplifier. The photocurrents were measured and normalized against a Hammamatsu Si photodiode reference, and long pass filters were used to block transmission of any stray secondary or tertiary diffractions outside of the range of interest. After completing the majority of the work presented in this paper, we found that due to the spectral mismatch of our solar simulator the photocurrents reported in this work were underestimated by approximately 25%. These lower values do not affect any conclusions in this paper; they further demonstrate the effectiveness of the ESSENCIAL fabrication method.

Morphology Characterization: The absorption spectra of polymer blend were measured using a Varian Cary 50 UV/Vis spectrophotometer. The weight ratio of PCBM to P3HT was calculated using Kratos Axis Ultra XPS results. PL spectra were obtained using PTI Quantamaster spectrofluorometer equipped with an integrating sphere. A Digital Instruments NanoScope IIIa-Phase atomic force microscope was used to obtain the AFM images.

Roll-to-Roll Process for Polymer PV Cells: The modified PDMS silicone sheet film was rolled around a nitrile rubber-coated nylon fabric belt, which was wrapped around two polytetrafluoroethylene (PTFE) rollers. Liquid-phase blend solution was continuously coated on the ITO substrate between the upper and lower rollers and the solvent evaporated through the gas-permeable silicone film while the roller pressure was applied. Web speed (10–20 mm s^{-1}) was controlled by an AC motor controller. Rolling force was measured in real-time by a flexible force sensor (Tekscan, Inc.) and adjusted by a clamping device. The squeezed flow behavior of the solution in the roll-to-roll process follows the dynamic elastic contact model, and the thickness of liquid coating is controlled by the solution concentration, roller pressure, and rolling speed.[30] The blend-film-coated ITO substrate separates from the silicone film continuously as the web moves forward. After 1 min heating at 130 °C, thermal deposition of LiF and Al completed devices.

Acknowledgements

This work was supported in part by the NSF, NIST, KACST, DOE, and a Rackham International Student Fellowship (HJP).

Received: January 21, 2010
Published online: April 26, 2010

[1] O. Morton, *Nature* **2006**, *443*, 19.
[2] N. S. Sariciftci, L. Smilowitz, A. J. Heeger, F. Wudl, *Science* **1992**, *258*, 1474.
[3] G. Yu, J. Gao, J. C. Hummelen, F. Wudl, A. J. Heeger, *Science* **1995**, *270*, 1789.
[4] J. J. M. Halls, C. A. Walsh, N. C. Greenham, E. A. Marseglia, R. H. Friend, S. C. Moratti, A. B. Holmes, *Nature* **1995**, *376*, 498.
[5] W. Ma, C. Yang, X. Gong, K. Lee, A. J. Heeger, *Adv. Funct. Mater.* **2005**, *16*, 1617.
[6] G. Li, V. Shrotriya, J. Huang, Y. Yao, T. Moriarty, K. Emery, Y. Yang, *Nat. Mater.* **2005**, *4*, 864.
[7] H.-Y. Chen, J. Hou, S. Zhang, Y. Liang, G. Yang, Y. Yang, L. Yu, Y. Wu, G. Li, *Nat. Photonics* **2009**, *3*, 649.
[8] F. C. Krebs, S. A. Gevorgyan, J. Alstrup, *J. Mater. Chem.* **2009**, *19*, 5442.
[9] F. C. Krebs, *Org. Electron.* **2009**, *10*, 761.
[10] L. Blankenburg, K. Schultheis, H. Schache, S. Sensfuss, M. Schrödner, *Sol. Energy Mater. Sol. Cells* **2009**, *93*, 476.
[11] S. S. van Bavel, E. Sourty, G. de With, J. Loos, *Nano Lett.* **2009**, *9*, 507.
[12] M. Campoy-Quiles, T. Ferenczi, T. Agostinelli, P. G. Etchegoin, Y. Kim, T. D. Anthopoulos, P. N. Stavrinou, D. D. C. Bradley, J. Nelson, *Nat. Mater.* **2008**, *7*, 158.
[13] Y. Yao, J. Hou, Z. Xu, G. Li, Y. Yang, *Adv. Funct. Mater.* **2008**, *18*, 1783.
[14] Z. Xu, L.-M. Chen, G. Yang, C.-H. Huang, J. Hou, Y. Wu, G. Li, C.-S. Hsu, Y. Yang, *Adv. Funct. Mater.* **2009**, *19*, 1227.
[15] D. S. Germack, C. K. Chan, B. H. Hamadani, L. J. Richter, D. A. Fischer, D. J. Gundlach, D. M. DeLongchamp, *Appl. Phys. Lett.* **2009**, *94*, 233303.
[16] A. Cravino, P. Schilinsky, C. J. Brabec, *Adv. Funct. Mater.* **2007**, *17*, 3906.
[17] M.-S. Kim, M.-G. Kang, L. J. Guo, J. Kim, *Appl. Phys. Lett.* **2008**, *92*, 133301.
[18] K. M. Coakley, M. D. McGehee, *Chem. Mater.* **2004**, *16*, 4533.
[19] S.-S. Kim, S.-I. Na, J. Jo, G. Tae, D.-Y. Kim, *Adv. Mater.* **2007**, *19*, 4410.
[20] M. Sunderberg, O. Inganas, S. Stafstrom, G. Gustafsson, B. Sjogren, *Solid State Commun.* **1989**, *71*, 435.
[21] V. D. Mihailetchi, L. J. A. Koster, P. W. M. Blom, C. Melzer, B. d. Boer, J. K. J. Duren, R. A. J. Janssen, *Adv. Funct. Mater.* **2005**, *15*, 795.
[22] V. Shrotriya, Y. Yao, G. Li, Y. Yang, *Appl. Phys. Lett.* **2006**, *89*, 063505.
[23] M. A. Lampert, P. Mark, in *Current Injection in Solids*, Academic Press, New York **1970**.
[24] A. Swinnen, I. Haeldermans, M. vande Ven, J. D'Haen, G. Vanhoyland, S. Aresu, M. D'Olieslaeger, J. Manca, *Adv. Funct. Mater.* **2006**, *16*, 760.
[25] J. Jo, S.-S. Kim, S.-I. Na, B.-K. Yu, D.-Y. Kim, *Adv. Funct. Mater.* **2009**, *19*, 866.
[26] Y. Kim, S. Cook, S. M. Tuladhar, S. A. Choulis, J. Nelson, J. R. Durrant, D. D. C. Bradley, M. Giles, I. Mcculloch, C.-S. Ha, M. Ree, *Nat. Mater.* **2006**, *5*, 197.
[27] G. Li, V. Shrotriya, Y. Yao, J. Huang, Y. Yang, *J. Mater. Chem.* **2007**, *17*, 3126.
[28] N. Koch, A. Elschner, R. L. Johnson, *J. Appl. Phys.* **2006**, *100*, 024512.
[29] M. D. Irwin, D. B. Buchholz, A. W. Hains, R. P. H. Chang, T. J. Marks, *Proc. Natl. Acad. Sci. USA* **2008**, *105*, 2783.
[30] S. H. Ahn, L. J. Guo, *ACS Nano* **2009**, *3*, 2304.
[31] C. Pina-Hernandez, J.-S. Kim, L. J. Guo, P.-F. Fu, *Adv. Mater.* **2007**, *19*, 1222.